1994A&A...283..319Z

Astron. Astrophys. 283, 319–330 (1994)

ASTRONOMY AND ASTROPHYSICS

Atomic data from the iron project

III. Rate coefficients for electron impact excitation of boron-like ions: Ne VI, Mg VIII, Al IX, Si X, S XII, Ar XIV, Ca XVI and Fe XXII*

Hong Lin Zhang, Mark Graziani, and Anil K. Pradhan

Department of Astronomy, Ohio State University, Columbus, Ohio 43210, USA

Received 14 May, accepted 16 August, 1993

Abstract. Collision strengths and maxwellian averaged rate coefficients have been calculated for the 105 transitions among all 15 fine structure levels of the 8 LS terms $2s^2 2p(^2P^0_{1/2,3/2})$, $2s2p^2(^4P_{1/2,3/2,5/2}, {}^2D_{3/2,5/2}, {}^2S_{1/2}, {}^2P_{1/2,3/2})$, $2p^3(^4S^0_{3/2}, {}^2D^0_{3/2,5/2}, {}^2P^0_{1/2,3/2})$ in highly-charged B-like Ne, Mg, Al, Si, S, Ar, Ca and Fe. Rate coefficients have been tabulated at a wide range of temperatures, depending on the ion charge and abundance in plasma sources. Earlier work for O IV (Blum & Pradhan 1992) has also been extended to include the high temperature range. A brief discussion of the calculations, sample results, and comparison with earlier works is also given. While much of the new data should be applicable to UV spectral diagnostics, the new rates for the important ground state fine structure transition $^2P^0_{1/2}$–$^2P^0_{3/2}$ should result in significant revision of the IR cooling rates in plasmas where B-like ions are prominent constituents, since the new rate coefficients are generally higher by several factors compared with the older data.

Key words: atomic data

1. Introduction

As part of the first phase of the Iron Project that deals with electron impact excitation of fine structure levels in ions along isoelectronic sequences (Hummer et al. 1993, hereafter Paper I), we present the results for the rate coefficients for B-like ions in this paper. Atomic data for highly charged B-like ions is of considerable interest in the study and modeling of high temperature astrophysical and laboratory plasmas. The spectra from ions in the Boron isoelectronic sequence is observed from a variety of astrophysical objects such as novae, planetary nebulae, Seyfert galaxies, the interstellar medium and the Sun. The spectral lines provide valuable temperature, density and abundance diagnostics in the UV and the IR region. The UV lines in the spectra of these ions emanate from transitions between the ground state levels $^2P^0_{1/2,3/2}$ and the higher levels ^4P_J, ^2D_J etc., whereas the IR lines are due to the transition within the fine structure levels of the ground state. Earlier work by Luo & Pradhan (1990) and Blum & Pradhan (1992) dealt with the calculation of collision strengths and rate coefficients for the first three members of the sequence, C II, N III, and O IV. However the rate coefficients were tabulated only up to a temperature of 40 000 K, which while appropriate for C II and N III is insufficient for O IV whose spectral formation may occur at much higher temperatures. In the present work therefore the work of Blum and Pradhan for O IV has been extended to $T > 40\,000$ K.

Apart from the R-matrix computations of Luo and Pradhan and Blum and Pradhan, previous calculations for B-like ions have been carried out by several workers. Hayes (1992) has reported close-coupling results for Ne VI in LS coupling including the 10 lowest LS terms. Saha & Trefftz (1982a, b) calculated collision data for several transitions in Si X and S XII from the lowest 2 levels to other higher levels using the close-coupling method; Zhang & Sampson (1993) recently calculated a large amount of collision strength data, also for the same transitions as in this work, in B-like ions with $8 \leq Z \leq 92$ using a fully relativistic distorted-wave method. This latter work did not include the coupling and resonance effects, which can be very important for some transitions, as discussed later.

In the present work, we have completed the work for the Boron-like ions of astrophysical interest, calculated using the R-matrix method and extended to include fine structure and relativistic effects. Collision strengths and rate coefficients are obtained for the 105 transitions among the 15 fine structure levels of the $n = 2$ complex for highly-charged B-like ions. The levels considered are: $2s^2 2p(^2P^0_{1/2,3/2})$, $2s2p^2(^4P_{1/2,3/2,5/2}, {}^2D_{3/2,5/2}, {}^2S_{1/2}, {}^2P_{1/2,3/2})$, $2p^3(^4S^0_{3/2}, {}^2D^0_{3/2,5/2}, {}^2P^0_{1/2,3/2})$. The present collision strength calculations involved an 8-term close-coupling expansion. The relativistic effects are included for Al IX, Si X, S XII,

Send offprint requests to: H.L. Zhang

* Tables for complete data for all ions are only avialable in electronic form: see the editorial in A&A 1992, Vol. 266 No. 2, page E1

© European Southern Observatory • Provided by the NASA Astrophysics Data System

1994A&A...283..319Z

Ar XIV, Ca XVI and Fe XXII using the term coupling formulation described by Eissner et al. (1974) and recently incorporated into the R-matrix codes. The Coulomb–Bethe approximation is employed to include the high partial-wave contributions for the optically allowed transitions. Maxwellian-averaged rate coefficients are tabulated for *scaled* electron temperatures between 100 and $50\,000z^2$ K, where the ion charge $z = Z - N$ with Z and N being the atomic number of the ion and the number of the electrons per ion, respectively. This temperature range is expected to cover the temperatures of abundance of the B-like ions as present in most plasma sources. A comparison of the results for Ne VI with those by Sampson et al. (1986), Hayes (1992) and Zhang & Sampson (1993) is also presented. The description of the R-matrix computer codes employed in the Iron Project is given in Paper I.

2. Atomic calculations

A detailed discussion of the method, as well as the results for C II, N III and O IV, is given in the earlier works by Luo and Pradhan (1990) and Blum and Pradhan (1992). The target data for the LS terms, such as the computed energy levels and the dipole oscillator strengths, is given by Luo & Pradhan (1989) for all the B-like ions treated in this work. The present work entails an extension to the highly charged members of the B-sequence in essentially the same manner as the earlier C, N, O work, but with the inclusion of relativistic effects for a number of ions. However, for Ne VI we have extended the calculations to include the $n = 3$ terms: $2s^23s, 3p, 3d(^2S, ^2P^0, ^2D)$, giving a 11-term target expansion, in order to make an accurate comparison with the earlier work by Hayes who included 10 terms, up to $2s^23p(^2P^0)$.

2.1. Resonances

As is well-known, the most important features of the close-coupling calculations are the inclusion of the strong coupling between the low-lying states of atoms and ions and the autoionizing resonances that generally enhance the effective scattering cross sections by a large amount, up to a factor of 2 or 3, or even more. The calculations are very extensive and require the collision strengths to be calculated at a large number of energies in order to delineate the resonances in detail. While it is sometimes believed that for more highly charged systems both the coupling and the resonance effects should be less important, this is often not the case, as seen in the present work.

For the highly charged ions the energies of the LS target terms of a given n-complex become relatively closer as the complexes themselves separate as z^2, but the terms within a complex separate only as z. Thus the resonances from the terms of a given complex simply move lower in energy as z^2, while the coupling effects between the corresponding terms may still remain relatively strong. Near the excitation threshold the effect of resonances could therefore still be appreciable, and consequently affect the rate coefficients at low temperatures. However, since the highly charged ions are abundant up to high temperatures, the effect of resonances may not be as significant in the higher temperature region.

In order to determine more precisely the effect of resonances due to higher complexes, we include the $n = 3$ complex of states in the calculations for Ne VI. The resonances due to the $n = 3$ terms are most likely to affect the rate coefficients of the high lying terms such as the $2p^3(^4S^0, ^2D^0, ^2P^0)$. In an earlier study on Ne VI, Hayes also included the $n = 3$ terms $2s^23s(^2S), 2s^23p(^2P^0)$, but not the $2S^23d(^2D)$. The present Ne VI calculations provide an estimate of the uncertainties in the collision strengths for high lying transitions to the $2p^3$ states for the other B-like ions.

As the resonances in the electron-ion scattering cross sections belong to a rydberg series, from low effective quantum numbers ν (usually 3.0–4.0) to infinity, we take account of the resonances in two ways: (i) for $\nu \leq \nu_{\max}$, the resonance structures are delineated in detail at 100 energies in each range $(\nu, \nu + 1)$, and (ii) resonance averaged collision strengths using the Gailitis averaging procedure for $\nu_{\max} < \nu < \infty$, as described in earlier works. The chosen value of $\nu_{\max}$ is usually taken to be 10.0; however we find that this is insufficient for highly charged ions since the range of the Gailitis averaging region expands as z^2 and it is necessary to increase $\nu_{\max}$ according to the effective charge on the scattering ion. We chose $\nu_{\max}$ to be 18.0, 20.0, 22.0, 24.0, 26.0, 28.0, 30.0 and 45.0 for Ne VI, Mg VIII, Al IX, Si X, S XII, Ar XIV, Ca XVI and Fe XXII, respectively. Although this procedure should result in greater accuracy in the rate coefficients, it does have the practical disadvantage that the number of electron energies for which the detailed collision strengths are to be calculated can be very large, from about 4000 to nearly 10 000.

Figure 1 illustrates the extensive resonance structures in the collision strengths for the important forbidden transition $^2P^0_{1/2} - ^2P^0_{3/2}$ in Ne VI, Si X, Ca XVI and Fe XXII. Although these are highly charged ions, the resonances significantly enhance the rate coefficients at low temperatures owing to the presence of a large number of near threshold autoionization features. For example, we find that the new rate coefficient for Ne VI is more than four times the previous value, 1.87 vs. 0.43 at 1000 K; the latter value was calculated in the distorted wave approximation neglecting resonance structures (Osterbrock 1989). The new rate coefficients for the ground state fine structure transition imply a significantly higher cooling rate in plasmas where B-like ions may be abundant.

2.2. Relativistic effects

The target representation for the B-like ions considered in this work is very similar to that for N III and O IV, as described in Luo & Pradhan (1990). The calculations include

© European Southern Observatory • Provided by the NASA Astrophysics Data System

1994A&A...283..319Z

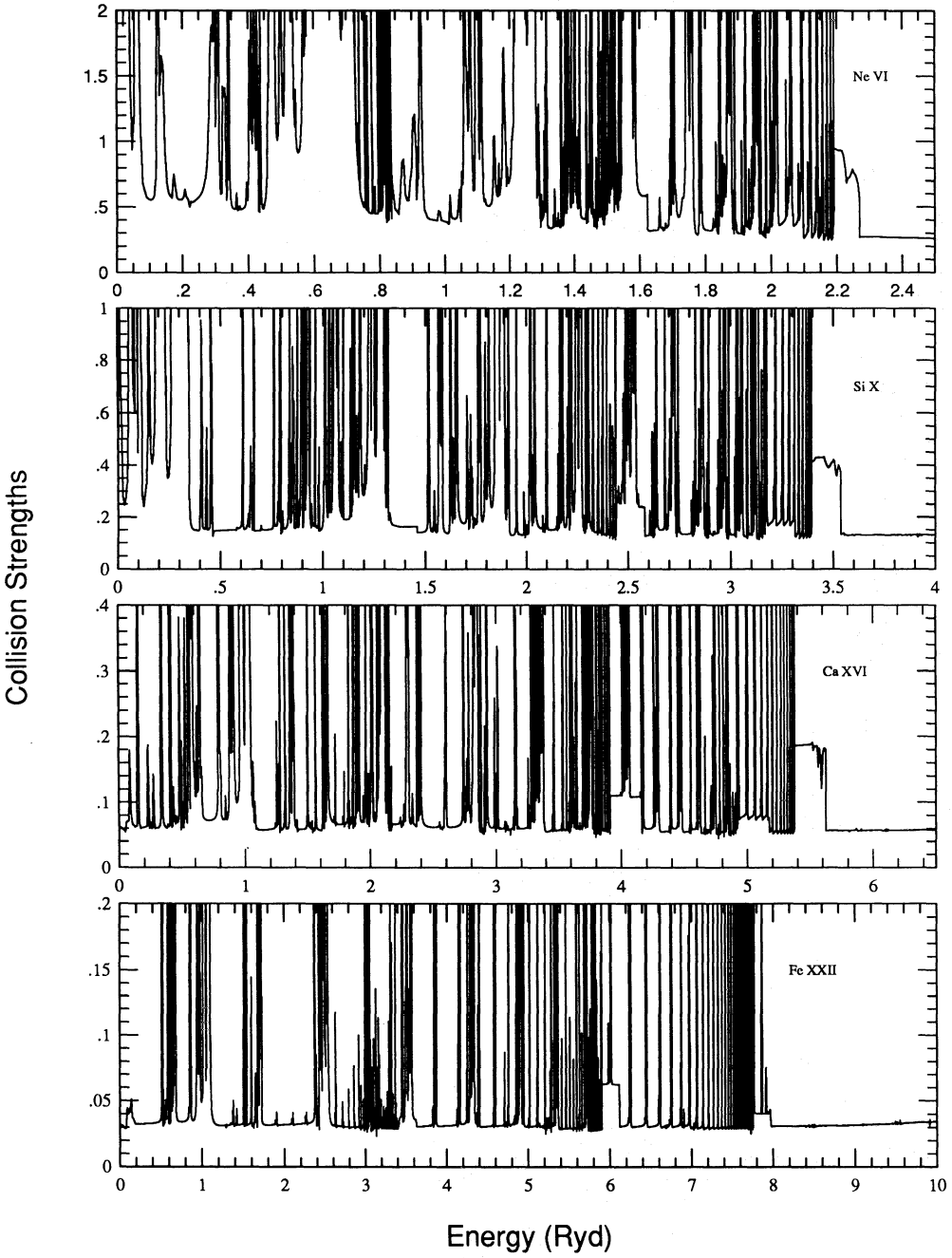

Fig. 1. The collision strengths for transition $^2P^0_{1/2}$–$^2P^0_{3/2}$ in Ne VI, Si X, Ca XVI and Fe XXII

8 terms with total LS symmetries: $2s^22p(^2P^0)$, $2s2p^2(^4P, ^2D, ^2S, ^2P)$ and $2p^3(^4S^0, ^2D^0, ^2P^0)$. These terms then split into 15 fine structure energy levels. The collision strength calculations were carried out using a revised and optimized version of the STGFJ code which is an extension of the asymptotic region code, STGF, of the non-relativistic (LS coupling) R-matrix package. The T-matrix elements are calculated in LS coupling and transformed to the pair-coupling representation to yield fine-structure collision strengths in STGFJ.

For heavier systems we expect the relativistic effects to manifest themselves in the fine structure collision strengths and it is more appropriate to switch to an intermediate coupling scheme. A useful procedure is to allow for term coupling between the fine structure levels of the target terms, as described by Eissner et al. (1974) and in Paper I (see,

© European Southern Observatory • Provided by the NASA Astrophysics Data System

1994A&A...283..319Z

for example, Pradhan 1983). These effects have been taken into account, via the term coupling formulation, for Al IX, Si X, S XII, Ar XIV, Ca XVI and Fe XXII.

2.3. Partial wave summation

The R-matrix calculations were carried out for all partial waves $0 \leq l \leq 9$, and associated total (electron + ion) symmetries $SL\pi$. While the collision strengths for the forbidden and the intercombination transitions converge for this range of partial waves, it is necessary to augment the summation with $l > 9$ for the dipole allowed transitions. In LS coupling the summation is easily carried out using the Burgess sum rule as described by Burke & Seaton (1986), and incorporated into the code STGF. For the fine structure collision strengths we employ the Coulomb–Bethe approximation to include contributions from higher partial waves at electron energies higher than the highest target threshold in the close coupling eigenfunction expansion. We have verified that the contributions to the collision strengths from $l > 9$ are negligible below the energy of the highest target threshold. The required electric dipole oscillator strengths, for all allowed fine structure transitions in the target, are calculated with the multi-configuration Dirac-Fock atomic structure code of Grant et al. (1980).

3. Rate coefficients

The maxwellian averaged collision strength, also known as the effective collision strength, is given by:

$$\Upsilon_{ij} = \int_0^\infty \Omega_{ij} e^{-\epsilon_j/kT} d(\epsilon_j/kT), \quad (1)$$

where Ω_{ij} is the collision strength for excitation from level i to level j, averaged over a maxwellian distribution of incident electron energies ϵ_j above the excitation threshold of the level j, at temperature T. This slowly varying function of temperature can then be used to obtain the rate coefficient, q_{ij}, for electron impact excitation,

$$q_{ij} = \frac{8.63\ 10^{-6}}{\sqrt{T} g_i} e^{-E_{ij}/kT} \Upsilon_{ij} \quad (\mathrm{cm^3\ s^{-1}}) \quad (2)$$

where E_{ij} is the energy difference between levels i and j and g_i is the statistical weight of level i.

Although we have carried out the calculations of maxwellian averaged collision strengths for all 105 transitions in each ion, in the present paper we present only the results for B-like O, Ne, Mg, Si and Fe, for some of the astrophysically important IR and UV transitions involving the levels $2s^2 2p(^2P^0_{1/2,3/2})$, $2s2p^2(^4P_{1/2,3/2,5/2}, ^2D_{3/2,5/2})$, as illustrative of the data calculated. The entire set of data (at a finer grid of temperatures) is available electronically on Internet by writing to the authors at:
zhang@payne.mps.ohio-state.edu

In Tables 1–5, we present the $\Upsilon_{ij}(T)$ for O IV, Ne VI, Mg VIII, Si X and Fe XXII respectively. The number key to the level indices, which appear as "Transition Keys" in Tables 1–5, is found in Table 6 which gives the corresponding spectroscopic fine structure energies for all 15 levels and all ions for which the data has been computed. We note that the level energies for Ne IV and Ar XIV are not all available from experimental data and are therefore taken from the Opacity Project data (a description of the data is provided in, for example, Seaton 1987, and Nahar & Pradhan 1991); for all of the remainder of the ions the level energies are the observed ones.

In the term coupling procedure employed in the present work to account for the relativistic effects, the fine structure energy splitting has not been taken into account in the collision strength calculations and the energy levels for the same LS term are treated as degenerate. Also, since the $^2S_{1/2}$ level for Fe XXII lies between the $^2P_{1/2}$ and the $^2P_{3/2}$, we use the weighted average of energies of these 2 terms and treat the 3 levels as degenerate. As the energies of the 3 levels are very close, this should not affect the Fe XXII results significantly.

It is convenient to divide the effective collision strength into two components, one from contributions of collision strengths at energies below the highest target threshold where autoionizing resonances are present, and the other from above this threshold where all channels are open and there are no resonances. The close-coupling method is highly accurate in the first region, but sometimes becomes less so for the second region where pseudo-resonances may appear in the collision strengths at higher energies and may thus serve to overestimate the effective collision strength. For low-lying transitions and lower temperatures, the effect of the pseudoresonances will be negligible on the rate coefficient. However, for transitions among high-lying states, especially those to the highest target threshold where the collision strength may be almost entirely in the region of all channels open, the effect of the pseudo-resonances can be significant (see Luo & Pradhan 1990).

In calculating effective collision strengths a search was made to detect pseudo-resonances and, when they were present, a linear interpolation was made to obtain values of collision strengths from the neighboring data points and to replace the collision strengths affected by pseudo-resonances. This results in a satisfactory energy behavior of the collision strengths in all energy regions and a smooth variation in the higher energy range.

4. Discussion

A detailed discussion of the present study of collision strengths for the entire Boron sequence will be given in a later publication (Zhang & Pradhan 1993). Here we briefly point out some salient features that are relevant to the calculations for the rate coefficients.

The present results have been compared with those by Hayes (1992) for Ne VI and by Zhang & Sampson (1993)

© European Southern Observatory • Provided by the NASA Astrophysics Data System

1994A&A...283..319Z

Table 1. Maxwellian-averaged collision strengths for O IV

Temp. (z^2 K)	Transition key								
	1 2 2 6 5 6	1 3 2 7 5 7	1 4 3 4 6 7	1 5 3 5	1 6 3 6	1 7 3 7	2 3 4 5	2 4 4 6	2 5 4 7
100.	1.61E+0	1.24E-1	1.84E-1	1.16E-1	1.56E+0	1.76E-1	8.81E-2	2.40E-1	5.20E-1
	5.24E-1	2.95E+0	1.01E+0	8.26E-1	3.58E-1	2.04E-1	2.15E+0	5.56E-1	5.68E-1
	4.35E-1	1.25E+0	3.39E+0						
500.	1.96E+0	1.20E-1	1.78E-1	1.13E-1	1.66E+0	2.84E-1	8.55E-2	2.33E-1	5.04E-1
	6.73E-1	3.22E+0	1.04E+0	7.23E-1	3.78E-1	2.20E-1	2.05E+0	5.89E-1	6.06E-1
	4.67E-1	1.32E+0	3.02E+0						
1000.	2.37E+0	1.31E-1	1.96E-1	1.32E-1	1.78E+0	4.91E-1	9.87E-2	2.62E-1	5.56E-1
	9.45E-1	3.59E+0	1.08E+0	6.85E-1	4.12E-1	2.40E-1	2.04E+0	6.42E-1	6.61E-1
	5.10E-1	1.44E+0	3.66E+0						
2000.	2.56E+0	1.46E-1	2.24E-1	1.65E-1	1.80E+0	6.24E-1	1.21E-1	3.11E-1	6.38E-1
	1.11E+0	3.73E+0	1.15E+0	7.24E-1	4.30E-1	2.54E-1	2.17E+0	6.73E-1	6.96E-1
	5.40E-1	1.51E+0	4.07E+0						
3000.	2.61E+0	1.53E-1	2.37E-1	1.82E-1	1.76E+0	6.23E-1	1.33E-1	3.35E-1	6.75E-1
	1.10E+0	3.67E+0	1.20E+0	7.75E-1	4.26E-1	2.55E-1	2.29E+0	6.68E-1	6.95E-1
	5.42E-1	1.50E+0	3.88E+0						
4000.	2.66E+0	1.54E-1	2.40E-1	1.88E-1	1.73E+0	5.93E-1	1.37E-1	3.42E-1	6.86E-1
	1.06E+0	3.59E+0	1.22E+0	8.08E-1	4.17E-1	2.54E-1	2.36E+0	6.55E-1	6.86E-1
	5.37E-1	1.47E+0	3.62E+0						
5000.	2.69E+0	1.53E-1	2.39E-1	1.89E-1	1.70E+0	5.59E-1	1.37E-1	3.42E-1	6.83E-1
	1.01E+0	3.51E+0	1.23E+0	8.26E-1	4.07E-1	2.50E-1	2.39E+0	6.42E-1	6.74E-1
	5.30E-1	1.44E+0	3.37E+0						
6000.	2.70E+0	1.51E-1	2.36E-1	1.86E-1	1.69E+0	5.27E-1	1.35E-1	3.38E-1	6.74E-1
	9.69E-1	3.45E+0	1.23E+0	8.35E-1	3.98E-1	2.47E-1	2.40E+0	6.28E-1	6.62E-1
	5.22E-1	1.41E+0	3.16E+0						
7000.	2.69E+0	1.48E-1	2.31E-1	1.83E-1	1.67E+0	4.97E-1	1.33E-1	3.31E-1	6.61E-1
	9.31E-1	3.40E+0	1.23E+0	8.36E-1	3.90E-1	2.43E-1	2.40E+0	6.15E-1	6.49E-1
	5.13E-1	1.38E+0	2.97E+0						
8000.	2.67E+0	1.45E-1	2.27E-1	1.78E-1	1.66E+0	4.71E-1	1.30E-1	3.24E-1	6.47E-1
	8.98E-1	3.36E+0	1.22E+0	8.34E-1	3.81E-1	2.39E-1	2.39E+0	6.03E-1	6.37E-1
	5.04E-1	1.36E+0	2.81E+0						
9000.	2.64E+0	1.42E-1	2.22E-1	1.74E-1	1.66E+0	4.48E-1	1.27E-1	3.17E-1	6.33E-1
	8.70E-1	3.32E+0	1.21E+0	8.29E-1	3.74E-1	2.35E-1	2.37E+0	5.91E-1	6.26E-1
	4.95E-1	1.33E+0	2.67E+0						
10000.	2.60E+0	1.39E-1	2.17E-1	1.69E-1	1.65E+0	4.28E-1	1.23E-1	3.09E-1	6.19E-1
	8.45E-1	3.30E+0	1.20E+0	8.22E-1	3.66E-1	2.31E-1	2.35E+0	5.79E-1	6.14E-1
	4.87E-1	1.30E+0	2.54E+0						
20000.	2.15E+0	1.16E-1	1.78E-1	1.34E-1	1.68E+0	3.06E-1	9.80E-2	2.50E-1	5.08E-1
	7.07E-1	3.22E+0	1.05E+0	7.21E-1	3.09E-1	1.96E-1	2.06E+0	4.90E-1	5.21E-1
	4.14E-1	1.10E+0	1.77E+0						
30000.	1.80E+0	1.01E-1	1.55E-1	1.13E-1	1.75E+0	2.50E-1	8.31E-2	2.14E-1	4.41E-1
	6.55E-1	3.28E+0	9.21E-1	6.36E-1	2.71E-1	1.73E-1	1.81E+0	4.29E-1	4.57E-1
	3.64E-1	9.66E-1	1.41E+0						
40000.	1.55E+0	9.16E-2	1.39E-1	9.92E-2	1.83E+0	2.17E-1	7.36E-2	1.91E-1	3.96E-1
	6.31E-1	3.37E+0	8.24E-1	5.74E-1	2.43E-1	1.56E-1	1.62E+0	3.86E-1	4.11E-1
	3.29E-1	8.68E-1	1.19E+0						
50000.	1.37E+0	8.45E-2	1.28E-1	9.00E-2	1.91E+0	1.95E-1	6.70E-2	1.74E-1	3.64E-1
	6.19E-1	3.48E+0	7.49E-1	5.28E-1	2.22E-1	1.44E-1	1.48E+0	3.53E-1	3.76E-1
	3.03E-1	7.94E-1	1.05E+0						

© European Southern Observatory • Provided by the NASA Astrophysics Data System

1994A&A...283..319Z

Table 2. Maxwellian-averaged collision strengths for Ne VI

Temp. (z^2 K) Transition key

	1 2 2 6 5 6	1 3 2 7 5 7	1 4 3 4 6 7	1 5 3 5	1 6 3 6	1 7 3 7	2 3 4 5	2 4 4 6	2 5 4 7
100.	3.71E+0	1.05E-1	1.93E-1	2.46E-1	1.05E+0	1.47E-1	1.67E-1	3.51E-1	5.71E-1
	3.87E-1	2.01E+0	6.68E-1	4.09E-1	4.96E-1	2.42E-1	1.25E+0	7.52E-1	7.26E-1
	5.25E-1	1.69E+0	6.41E+0						
500.	3.05E+0	8.56E-2	1.41E-1	1.34E-1	1.18E+0	3.00E-1	9.45E-2	2.20E-1	4.06E-1
	5.99E-1	2.36E+0	5.96E-1	4.14E-1	2.91E-1	1.67E-1	1.17E+0	4.53E-1	4.63E-1
	3.55E-1	1.02E+0	4.20E+0						
1000.	2.40E+0	8.90E-2	1.45E-1	1.34E-1	1.20E+0	3.34E-1	9.48E-2	2.23E-1	4.17E-1
	6.46E-1	2.42E+0	6.80E-1	4.86E-1	2.50E-1	1.52E-1	1.36E+0	3.93E-1	4.11E-1
	3.21E-1	8.85E-1	3.16E+0						
2000.	2.14E+0	8.87E-2	1.43E-1	1.29E-1	1.16E+0	3.05E-1	9.19E-2	2.18E-1	4.12E-1
	6.02E-1	2.32E+0	7.57E-1	5.39E-1	2.22E-1	1.42E-1	1.51E+0	3.53E-1	3.75E-1
	2.99E-1	7.94E-1	2.39E+0						
3000.	2.05E+0	8.40E-2	1.35E-1	1.20E-1	1.12E+0	2.67E-1	8.55E-2	2.04E-1	3.88E-1
	5.51E-1	2.23E+0	7.59E-1	5.35E-1	2.06E-1	1.34E-1	1.50E+0	3.28E-1	3.51E-1
	2.81E-1	7.37E-1	2.04E+0						
4000.	1.96E+0	7.88E-2	1.26E-1	1.10E-1	1.11E+0	2.37E-1	7.89E-2	1.89E-1	3.62E-1
	5.10E-1	2.17E+0	7.40E-1	5.17E-1	1.93E-1	1.26E-1	1.46E+0	3.07E-1	3.30E-1
	2.65E-1	6.91E-1	1.82E+0						
5000.	1.88E+0	7.40E-2	1.18E-1	1.02E-1	1.10E+0	2.13E-1	7.30E-2	1.76E-1	3.38E-1
	4.80E-1	2.13E+0	7.13E-1	4.96E-1	1.82E-1	1.19E-1	1.40E+0	2.90E-1	3.12E-1
	2.50E-1	6.52E-1	1.65E+0						
6000.	1.79E+0	6.97E-2	1.11E-1	9.46E-2	1.10E+0	1.94E-1	6.80E-2	1.64E-1	3.18E-1
	4.57E-1	2.11E+0	6.86E-1	4.74E-1	1.73E-1	1.13E-1	1.35E+0	2.75E-1	2.95E-1
	2.37E-1	6.19E-1	1.51E+0						
7000.	1.71E+0	6.61E-2	1.04E-1	8.82E-2	1.10E+0	1.79E-1	6.37E-2	1.54E-1	3.00E-1
	4.39E-1	2.10E+0	6.58E-1	4.53E-1	1.64E-1	1.07E-1	1.29E+0	2.62E-1	2.81E-1
	2.26E-1	5.89E-1	1.40E+0						
8000.	1.63E+0	6.30E-2	9.88E-2	8.28E-2	1.11E+0	1.66E-1	6.00E-2	1.45E-1	2.84E-1
	4.26E-1	2.10E+0	6.33E-1	4.34E-1	1.57E-1	1.03E-1	1.24E+0	2.51E-1	2.69E-1
	2.16E-1	5.64E-1	1.31E+0						
9000.	1.55E+0	6.03E-2	9.41E-2	7.81E-2	1.12E+0	1.56E-1	5.68E-2	1.38E-1	2.71E-1
	4.15E-1	2.11E+0	6.09E-1	4.16E-1	1.51E-1	9.86E-2	1.19E+0	2.41E-1	2.59E-1
	2.07E-1	5.42E-1	1.23E+0						
10000.	1.48E+0	5.80E-2	9.00E-2	7.40E-2	1.13E+0	1.47E-1	5.40E-2	1.31E-1	2.59E-1
	4.07E-1	2.11E+0	5.87E-1	4.01E-1	1.46E-1	9.49E-2	1.15E+0	2.32E-1	2.49E-1
	2.00E-1	5.22E-1	1.16E+0						
20000.	1.03E+0	4.63E-2	6.68E-2	5.14E-2	1.25E+0	1.02E-1	3.88E-2	9.46E-2	1.94E-1
	3.78E-1	2.27E+0	4.44E-1	3.01E-1	1.13E-1	7.28E-2	8.68E-1	1.79E-1	1.92E-1
	1.53E-1	4.04E-1	7.73E-1						
30000.	8.11E-1	4.19E-2	5.68E-2	4.18E-2	1.35E+0	8.34E-2	3.22E-2	7.89E-2	1.66E-1
	3.79E-1	2.43E+0	3.71E-1	2.55E-1	9.66E-2	6.20E-2	7.29E-1	1.53E-1	1.64E-1
	1.31E-1	3.45E-1	6.08E-1						
40000.	6.79E-1	3.90E-2	5.09E-2	3.63E-2	1.44E+0	7.30E-2	2.82E-2	6.98E-2	1.49E-1
	3.85E-1	2.58E+0	3.25E-1	2.29E-1	8.60E-2	5.51E-2	6.45E-1	1.36E-1	1.46E-1
	1.16E-1	3.07E-1	5.15E-1						
50000.	5.92E-1	3.67E-2	4.66E-2	3.26E-2	1.52E+0	6.58E-2	2.55E-2	6.34E-2	1.37E-1
	3.92E-1	2.71E+0	2.92E-1	2.11E-1	7.82E-2	5.01E-2	5.86E-1	1.24E-1	1.33E-1
	1.06E-1	2.79E-1	4.55E-1						

© European Southern Observatory • Provided by the NASA Astrophysics Data System

1994A&A...283..319Z

Table 3. Maxwellian-averaged collision strengths for Mg VIII

Temp. (z^2 K)	Transition key								
	1 2 2 6 5 6	1 3 2 7 5 7	1 4 3 4 6 7	1 5 3 5	1 6 3 6	1 7 3 7	2 3 4 5	2 4 4 6	2 5 4 7
100.	8.52E-1	4.26E-2	6.36E-2	4.10E-2	9.72E-1	3.08E-1	3.10E-2	8.40E-2	1.80E-1
	5.64E-1	1.99E+0	3.18E-1	2.21E-1	1.08E-1	6.80E-2	6.26E-1	1.71E-1	1.81E-1
	1.44E-1	3.85E-1	1.06E+0						
500.	1.06E+0	5.61E-2	9.01E-2	7.55E-2	9.01E-1	2.27E-1	5.45E-2	1.33E-1	2.59E-1
	4.54E-1	1.79E+0	3.20E-1	2.24E-1	1.17E-1	7.16E-2	6.33E-1	1.85E-1	1.93E-1
	1.52E-1	4.16E-1	1.75E+0						
1000.	1.00E+0	5.53E-2	8.96E-2	7.71E-2	8.55E-1	1.98E-1	5.54E-2	1.34E-1	2.58E-1
	4.10E-1	1.69E+0	3.77E-1	2.69E-1	1.12E-1	7.01E-2	7.51E-1	1.77E-1	1.87E-1
	1.48E-1	3.99E-1	1.53E+0						
2000.	1.04E+0	5.02E-2	8.09E-2	6.92E-2	8.10E-1	1.57E-1	4.97E-2	1.20E-1	2.33E-1
	3.52E-1	1.57E+0	4.18E-1	2.95E-1	1.05E-1	6.64E-2	8.29E-1	1.66E-1	1.76E-1
	1.40E-1	3.73E-1	1.23E+0						
3000.	1.04E+0	4.57E-2	7.31E-2	6.14E-2	7.94E-1	1.31E-1	4.42E-2	1.08E-1	2.10E-1
	3.17E-1	1.52E+0	4.17E-1	2.92E-1	9.86E-2	6.27E-2	8.24E-1	1.56E-1	1.66E-1
	1.32E-1	3.52E-1	1.05E+0						
4000.	1.01E+0	4.22E-2	6.71E-2	5.52E-2	7.92E-1	1.14E-1	3.99E-2	9.79E-2	1.93E-1
	2.96E-1	1.50E+0	4.04E-1	2.80E-1	9.37E-2	5.96E-2	7.95E-1	1.49E-1	1.58E-1
	1.26E-1	3.34E-1	9.19E-1						
5000.	9.63E-1	3.94E-2	6.24E-2	5.04E-2	7.96E-1	1.02E-1	3.65E-2	9.02E-2	1.79E-1
	2.82E-1	1.49E+0	3.87E-1	2.67E-1	8.97E-2	5.69E-2	7.59E-1	1.42E-1	1.51E-1
	1.20E-1	3.20E-1	8.23E-1						
6000.	9.14E-1	3.73E-2	5.86E-2	4.65E-2	8.04E-1	9.32E-2	3.38E-2	8.42E-2	1.68E-1
	2.73E-1	1.49E+0	3.70E-1	2.54E-1	8.63E-2	5.47E-2	7.24E-1	1.37E-1	1.45E-1
	1.15E-1	3.08E-1	7.48E-1						
7000.	8.66E-1	3.55E-2	5.56E-2	4.34E-2	8.14E-1	8.62E-2	3.17E-2	7.93E-2	1.59E-1
	2.66E-1	1.50E+0	3.54E-1	2.42E-1	8.34E-2	5.28E-2	6.92E-1	1.32E-1	1.40E-1
	1.11E-1	2.97E-1	6.88E-1						
8000.	8.22E-1	3.41E-2	5.31E-2	4.09E-2	8.25E-1	8.07E-2	2.99E-2	7.52E-2	1.52E-1
	2.61E-1	1.51E+0	3.39E-1	2.31E-1	8.08E-2	5.11E-2	6.62E-1	1.28E-1	1.36E-1
	1.08E-1	2.88E-1	6.38E-1						
9000.	7.81E-1	3.28E-2	5.10E-2	3.88E-2	8.36E-1	7.61E-2	2.84E-2	7.18E-2	1.46E-1
	2.58E-1	1.53E+0	3.25E-1	2.22E-1	7.85E-2	4.96E-2	6.36E-1	1.24E-1	1.32E-1
	1.05E-1	2.80E-1	5.96E-1						
10000.	7.44E-1	3.17E-2	4.91E-2	3.69E-2	8.48E-1	7.23E-2	2.71E-2	6.89E-2	1.40E-1
	2.55E-1	1.54E+0	3.13E-1	2.14E-1	7.65E-2	4.83E-2	6.12E-1	1.21E-1	1.28E-1
	1.02E-1	2.72E-1	5.61E-1						
20000.	5.14E-1	2.56E-2	3.88E-2	2.70E-2	9.52E-1	5.27E-2	2.02E-2	5.27E-2	1.10E-1
	2.49E-1	1.69E+0	2.36E-1	1.65E-1	6.29E-2	3.95E-2	4.66E-1	9.94E-2	1.05E-1
	8.33E-2	2.24E-1	3.72E-1						
30000.	4.05E-1	2.24E-2	3.37E-2	2.26E-2	1.03E+0	4.44E-2	1.70E-2	4.51E-2	9.57E-2
	2.52E-1	1.82E+0	1.98E-1	1.43E-1	5.49E-2	3.44E-2	3.96E-1	8.68E-2	9.18E-2
	7.27E-2	1.95E-1	2.94E-1						
40000.	3.41E-1	2.03E-2	3.03E-2	1.98E-2	1.10E+0	3.93E-2	1.50E-2	4.01E-2	8.59E-2
	2.57E-1	1.92E+0	1.73E-1	1.30E-1	4.92E-2	3.08E-2	3.53E-1	7.78E-2	8.23E-2
	6.51E-2	1.75E-1	2.51E-1						
50000.	2.99E-1	1.86E-2	2.76E-2	1.78E-2	1.15E+0	3.55E-2	1.35E-2	3.64E-2	7.84E-2
	2.61E-1	2.01E+0	1.55E-1	1.21E-1	4.48E-2	2.81E-2	3.22E-1	7.08E-2	7.50E-2
	5.93E-2	1.59E-1	2.23E-1						

© European Southern Observatory • Provided by the NASA Astrophysics Data System

1994A&A...283..319Z

Table 4. Maxwellian-averaged collision strengths for Si X

Temp. (z^2 K)	Transition key								
	1 2 2 6 5 6	1 3 2 7 5 7	1 4 3 4 6 7	1 5 3 5	1 6 3 6	1 7 3 7	2 3 4 5	2 4 4 6	2 5 4 7
100.	1.14E+0 2.17E-1 8.64E-2	3.30E-2 1.16E+0 2.40E-1	5.05E-2 1.63E-1 1.69E+0	3.55E-2 7.12E-2	6.16E-1 6.59E-2	7.24E-2 3.89E-2	2.63E-2 2.68E-1	6.97E-2 1.03E-1	1.44E-1 1.09E-1
500.	1.57E+0 2.82E-1 1.04E-1	4.03E-2 1.30E+0 2.68E-1	6.43E-2 1.93E-1 1.15E+0	5.25E-2 1.08E-1	6.71E-1 7.30E-2	1.15E-1 4.72E-2	3.79E-2 3.50E-1	9.59E-2 1.16E-1	1.85E-1 1.27E-1
1000.	1.36E+0 2.68E-1 1.02E-1	3.79E-2 1.23E+0 2.60E-1	6.07E-2 2.34E-1 9.84E-1	5.06E-2 1.51E-1	6.33E-1 7.05E-2	1.09E-1 4.64E-2	3.64E-2 4.55E-1	9.06E-2 1.13E-1	1.74E-1 1.23E-1
2000.	1.14E+0 2.36E-1 9.31E-2	3.27E-2 1.13E+0 2.38E-1	5.22E-2 2.57E-1 7.90E-1	4.34E-2 1.77E-1	5.88E-1 6.47E-2	8.53E-2 4.22E-2	3.11E-2 5.13E-1	7.71E-2 1.03E-1	1.50E-1 1.13E-1
3000.	1.01E+0 2.18E-1 8.61E-2	2.90E-2 1.10E+0 2.21E-1	4.60E-2 2.50E-1 6.67E-1	3.76E-2 1.74E-1	5.74E-1 6.04E-2	7.08E-2 3.89E-2	2.70E-2 5.00E-1	6.71E-2 9.61E-2	1.32E-1 1.04E-1
4000.	9.01E-1 2.09E-1 8.09E-2	2.64E-2 1.09E+0 2.09E-1	4.16E-2 2.37E-1 5.79E-1	3.34E-2 1.66E-1	5.73E-1 5.71E-2	6.14E-2 3.65E-2	2.41E-2 4.74E-1	6.01E-2 9.08E-2	1.19E-1 9.82E-2
5000.	8.16E-1 2.03E-1 7.69E-2	2.45E-2 1.09E+0 1.99E-1	3.84E-2 2.24E-1 5.14E-1	3.03E-2 1.57E-1	5.79E-1 5.45E-2	5.50E-2 3.46E-2	2.19E-2 4.47E-1	5.49E-2 8.66E-2	1.09E-1 9.34E-2
6000.	7.47E-1 2.00E-1 7.36E-2	2.30E-2 1.10E+0 1.91E-1	3.60E-2 2.12E-1 4.64E-1	2.80E-2 1.49E-1	5.88E-1 5.24E-2	5.03E-2 3.31E-2	2.03E-2 4.22E-1	5.09E-2 8.31E-2	1.02E-1 8.95E-2
7000.	6.88E-1 1.98E-1 7.08E-2	2.19E-2 1.11E+0 1.84E-1	3.40E-2 2.01E-1 4.24E-1	2.61E-2 1.41E-1	5.98E-1 5.06E-2	4.66E-2 3.18E-2	1.90E-2 4.01E-1	4.78E-2 8.02E-2	9.66E-2 8.62E-2
8000.	6.39E-1 1.97E-1 6.84E-2	2.09E-2 1.13E+0 1.79E-1	3.24E-2 1.92E-1 3.91E-1	2.46E-2 1.35E-1	6.09E-1 4.90E-2	4.38E-2 3.07E-2	1.79E-2 3.82E-1	4.52E-2 7.76E-2	9.20E-2 8.34E-2
9000.	5.97E-1 1.96E-1 6.63E-2	2.01E-2 1.14E+0 1.73E-1	3.11E-2 1.84E-1 3.64E-1	2.33E-2 1.30E-1	6.19E-1 4.76E-2	4.14E-2 2.97E-2	1.70E-2 3.66E-1	4.31E-2 7.54E-2	8.81E-2 8.08E-2
10000.	5.61E-1 1.95E-1 6.45E-2	1.94E-2 1.16E+0 1.69E-1	2.99E-2 1.77E-1 3.42E-1	2.22E-2 1.25E-1	6.29E-1 4.63E-2	3.95E-2 2.89E-2	1.63E-2 3.52E-1	4.13E-2 7.34E-2	8.48E-2 7.86E-2
20000.	3.63E-1 1.97E-1 5.26E-2	1.56E-2 1.28E+0 1.37E-1	2.35E-2 1.33E-1 2.24E-1	1.64E-2 9.76E-2	7.14E-1 3.80E-2	2.92E-2 2.35E-2	1.23E-2 2.68E-1	3.15E-2 6.01E-2	6.65E-2 6.34E-2
30000.	2.79E-1 2.00E-1 4.58E-2	1.36E-2 1.38E+0 1.18E-1	2.03E-2 1.11E-1 1.77E-1	1.38E-2 8.58E-2	7.75E-1 3.31E-2	2.46E-2 2.05E-2	1.05E-2 2.30E-1	2.69E-2 5.23E-2	5.74E-2 5.46E-2
40000.	2.33E-1 2.02E-1 4.10E-2	1.23E-2 1.45E+0 1.04E-1	1.81E-2 9.78E-2 1.51E-1	1.21E-2 7.89E-2	8.23E-1 2.96E-2	2.17E-2 1.84E-2	9.28E-3 2.06E-1	2.38E-2 4.68E-2	5.13E-2 4.84E-2
50000.	2.03E-1 2.04E-1 3.73E-2	1.12E-2 1.52E+0 9.44E-2	1.65E-2 8.79E-2 1.34E-1	1.09E-2 7.44E-2	8.63E-1 2.69E-2	1.96E-2 1.68E-2	8.42E-3 1.89E-1	2.16E-2 4.25E-2	4.67E-2 4.37E-2

© European Southern Observatory • Provided by the NASA Astrophysics Data System

1994A&A...283..319Z

Table 5. Maxwellian-averaged collision strengths for Fe XXII

Temp. (z^2 K)	Transition key								
	1 2 2 6 5 6	1 3 2 7 5 7	1 4 3 4 6 7	1 5 3 5	1 6 3 6	1 7 3 7	2 3 4 5	2 4 4 6	2 5 4 7
100.	5.66E-2	4.49E-3	6.98E-3	5.47E-3	1.77E-1	4.76E-2	3.98E-3	9.96E-3	1.99E-2
	9.95E-2	3.38E-1	1.24E-1	8.68E-2	1.20E-2	6.89E-3	2.45E-1	2.00E-2	2.60E-2
	2.16E-2	7.62E-2	1.18E-1						
500.	1.34E-1	5.18E-3	8.17E-3	7.30E-3	1.38E-1	2.65E-2	5.00E-3	1.19E-2	2.52E-2
	8.54E-2	2.79E-1	7.56E-2	5.32E-2	1.20E-2	7.11E-3	1.50E-1	2.01E-2	2.45E-2
	2.38E-2	7.94E-2	1.48E-1						
1000.	1.36E-1	5.44E-3	7.60E-3	6.70E-3	1.23E-1	1.74E-2	4.67E-3	1.04E-2	2.54E-2
	8.71E-2	2.62E-1	6.14E-2	4.38E-2	1.16E-2	7.17E-3	1.22E-1	1.86E-2	2.27E-2
	2.16E-2	6.99E-2	1.16E-1						
2000.	1.13E-1	6.36E-3	7.02E-3	5.88E-3	1.24E-1	1.13E-2	4.66E-3	8.89E-3	2.59E-2
	9.06E-2	2.67E-1	4.80E-2	3.48E-2	1.09E-2	6.93E-3	9.53E-2	1.70E-2	2.06E-2
	1.90E-2	5.99E-2	8.43E-2						
3000.	9.59E-2	7.16E-3	6.75E-3	5.45E-3	1.34E-1	8.97E-3	4.82E-3	8.29E-3	2.66E-2
	9.25E-2	2.79E-1	4.11E-2	3.02E-2	1.05E-2	6.72E-3	8.18E-2	1.61E-2	1.95E-2
	1.75E-2	5.46E-2	6.83E-2						
4000.	8.39E-2	7.77E-3	6.59E-3	5.18E-3	1.44E-1	7.72E-3	4.98E-3	7.98E-3	2.73E-2
	9.35E-2	2.91E-1	3.69E-2	2.73E-2	1.02E-2	6.55E-3	7.36E-2	1.55E-2	1.88E-2
	1.66E-2	5.12E-2	5.88E-2						
5000.	7.53E-2	8.24E-3	6.47E-3	4.99E-3	1.54E-1	6.94E-3	5.11E-3	7.79E-3	2.80E-2
	9.38E-2	3.02E-1	3.40E-2	2.54E-2	9.99E-3	6.43E-3	6.80E-2	1.51E-2	1.83E-2
	1.59E-2	4.88E-2	5.24E-2						
6000.	6.90E-2	8.61E-3	6.37E-3	4.84E-3	1.63E-1	6.42E-3	5.23E-3	7.66E-3	2.85E-2
	9.38E-2	3.12E-1	3.18E-2	2.40E-2	9.81E-3	6.32E-3	6.39E-2	1.49E-2	1.80E-2
	1.54E-2	4.69E-2	4.79E-2						
7000.	6.40E-2	8.91E-3	6.28E-3	4.71E-3	1.71E-1	6.03E-3	5.32E-3	7.56E-3	2.89E-2
	9.35E-2	3.20E-1	3.01E-2	2.29E-2	9.65E-3	6.24E-3	6.06E-2	1.46E-2	1.77E-2
	1.50E-2	4.54E-2	4.45E-2						
8000.	6.01E-2	9.16E-3	6.19E-3	4.60E-3	1.78E-1	5.73E-3	5.39E-3	7.48E-3	2.92E-2
	9.31E-2	3.28E-1	2.87E-2	2.20E-2	9.51E-3	6.16E-3	5.80E-2	1.45E-2	1.74E-2
	1.46E-2	4.41E-2	4.18E-2						
9000.	5.69E-2	9.37E-3	6.11E-3	4.51E-3	1.85E-1	5.49E-3	5.45E-3	7.40E-3	2.95E-2
	9.25E-2	3.35E-1	2.75E-2	2.13E-2	9.38E-3	6.09E-3	5.59E-2	1.43E-2	1.72E-2
	1.43E-2	4.30E-2	3.96E-2						
10000.	5.42E-2	9.55E-3	6.03E-3	4.42E-3	1.91E-1	5.28E-3	5.51E-3	7.34E-3	2.98E-2
	9.19E-2	3.41E-1	2.65E-2	2.07E-2	9.25E-3	6.03E-3	5.40E-2	1.41E-2	1.70E-2
	1.40E-2	4.20E-2	3.78E-2						
20000.	4.00E-2	1.05E-2	5.35E-3	3.75E-3	2.35E-1	4.12E-3	5.76E-3	6.86E-3	3.11E-2
	8.50E-2	3.87E-1	2.06E-2	1.72E-2	8.06E-3	5.53E-3	4.36E-2	1.23E-2	1.49E-2
	1.18E-2	3.50E-2	2.84E-2						
30000.	3.37E-2	1.10E-2	4.83E-3	3.29E-3	2.62E-1	3.48E-3	5.84E-3	6.50E-3	3.15E-2
	7.90E-2	4.16E-1	1.75E-2	1.56E-2	7.11E-3	5.17E-3	3.85E-2	1.08E-2	1.32E-2
	1.03E-2	3.07E-2	2.43E-2						
40000.	2.99E-2	1.11E-2	4.42E-3	2.94E-3	2.80E-1	3.04E-3	5.85E-3	6.20E-3	3.16E-2
	7.40E-2	4.33E-1	1.54E-2	1.44E-2	6.36E-3	4.88E-3	3.51E-2	9.59E-3	1.18E-2
	9.18E-3	2.75E-2	2.18E-2						
50000.	2.71E-2	1.11E-2	4.07E-3	2.65E-3	2.89E-1	2.70E-3	5.79E-3	5.92E-3	3.13E-2
	6.97E-2	4.41E-1	1.38E-2	1.36E-2	5.76E-3	4.63E-3	3.25E-2	8.61E-3	1.07E-2
	8.32E-3	2.50E-2	1.99E-2						

© European Southern Observatory • Provided by the NASA Astrophysics Data System

1994A&A...283..319Z

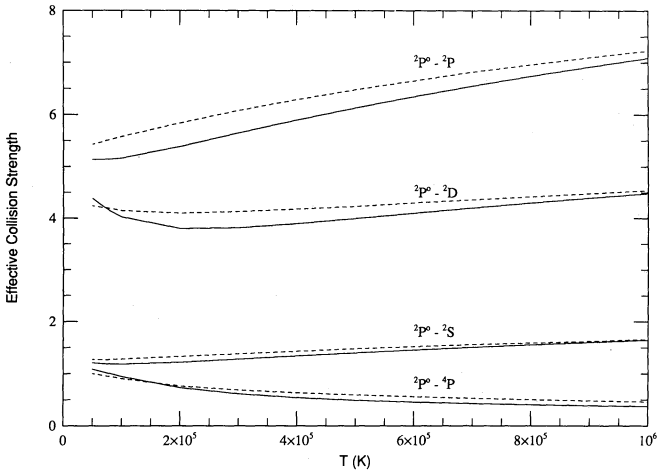

Fig. 2. Comparison of the present effective collision strengths with those by Hayes (1992) for transitions $^2P^0$–^2P, $^2P^0$–^2D, $^2P^0$–^2S and $^2P^0$–^4P in Ne VI. The solid lines: the present results; the dashed lines: Hayes's results

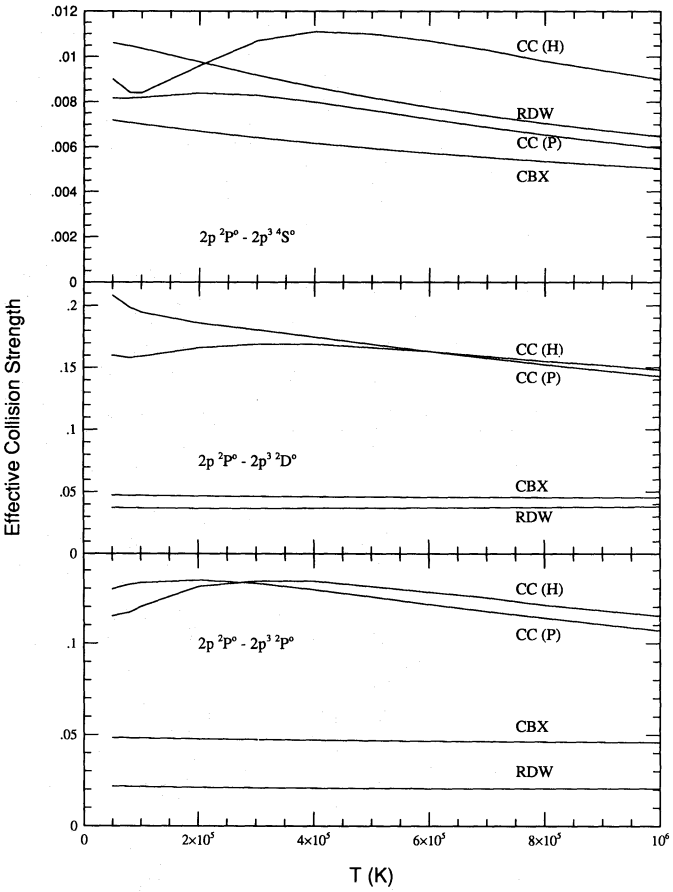

Fig. 3. Comparison of the present effective collision strengths with other works for transitions from $2p^2P^0$ to $2p^3\ ^4S^0$, $2p^3\ ^2D^0$ and $2p^3\ ^2P^0$ in Ne VI. CC(P) indicates the present results, CC(H) those by Hayes (1992), RDW those by Zhang & Sampson (1993) and CBX the Coulomb-Born-exchange results by Sampson et al. (1986)

for all the B-like ions. For transitions among the low-lying levels the agreement is usually good between all three sets of calculations. The Zhang and Sampson work does not include the resonances but is in reasonable agreement with the close coupling values for the background, non-resonant collision strengths for the low-lying transitions. The agreement with Hayes's results for these transitions is also good. For example, Fig. 2 gives a comparison of effective collision strengths for $^2P^0$–^2P, $^2P^0$–^2D, $^2P^0$–^2S and $^2P^0$–^4P transitions in Ne VI, between the present results and those of Hayes (1992).

For transitions to levels higher than the $2s2p^2$ terms, i.e. the terms $^4S^0$, $^2D^0$, $^2P^0$ dominated by $2p^3$, we find larger uncertainties in the different sets of data, but our values agree reasonably well with those of Hayes (1992). Figure 3 shows a comparison of the present collision strengths (summed over the fine structure), for the excitation from the ground state $^2P^0$ to the three $2p^3$ terms, with previous calculations: Coulomb-Born with exchange (CBX) by Sampson et al. (1986), the relativistic distorted wave (RDW) by Zhang & Sampson (1993), and the close coupling calculations by Hayes (1992). The rather large rise in the values for the $2s^22p(^2P^0)$–$2p^3(^4S^0)$ transition seen by Hayes at low temperatures may be due to the exclusion of the $2s^23d$ configuration, possibly giving rise to a $3d^2$ type pseudoresonance in the collision strengths.

A more detailed study (Zhang & Pradhan 1993) enables us to place the following approximate error estimates on the maxwellian averaged collision strengths in Tables 1–5. For the important transitions among levels that lie fairly low in the close-coupling expansion, the collision strengths and, consequently the rate coefficients, should be accurate to approximately 20%. For excitations to levels lying higher than the $2s2p^2(^4P)$ state, the uncertainties in the rate coefficients could be 30–50%; the degradation in accuracy generally follows the excitation energy of the upper level. Although the effect of resonances due to the $n = 3$ complex of states should decrease with ion charge, the Ne VI results including those states show that the present rate coefficients for the $2p^3(^4S^0, ^2D^0, ^2P^0)$ terms may have been somewhat underestimated for the other ions (although within the uncertainty estimates given above).

It is also noted that the relativistic effects start to be non-negligible for some transitions when $Z \geq 20$, especially for transitions involving those energy levels that have switched energy order compared with neighboring Z-ions. These effects are significant for some transitions in Fe XXII, as seen for example in Fig. 4, which shows the collision strength for the transition $^2P^0_{1/2}$– $^4P_{1/2}$ within the important intercombination multiplet $^2P^0$–^4P. Intercombination transitions are usually most affected by the relativistic mixing between the forbidden and the allowed transitions owing to the departure from pure LS coupling. For this transition in Fe XXII the rate coefficients with and without term coupling coefficients

© European Southern Observatory • Provided by the NASA Astrophysics Data System

1994A&A...283..319Z

Table 6. Level indices and energies in rydbergs

Level	Designation	Ne IV	Mg VIII	Al IX	Si X	S XII	Ar XVI	Ca XVI	Fe XXII
1	$2s^2 2p\ ^2P^o_{1/2}$	0.000000	0.000000	0.000000	0.000000	0.000000	0.000000	0.000000	0.000000
2	$2s^2 2p\ ^2P^o_{3/2}$	0.011900	0.030090	0.044561	0.063703	0.119698	0.208725	0.332795	1.077756
3	$2s2p^2\ ^4P_{1/2}$	0.913600	1.183645	1.323798	1.467231	1.766783	2.083269	2.442105	3.686531
4	$2s2p^2\ ^4P_{3/2}$	0.917600	1.194033	1.339472	1.489831	1.810460	2.162855	2.574330	4.193651
5	$2s2p^2\ ^4P_{5/2}$	0.923500	1.209343	1.361980	1.522363	1.871970	2.275590	2.741091	4.677170
6	$2s2p^2\ ^2D_{3/2}$	1.631100	2.116937	2.367107	2.623082	3.159363	3.772033	4.368797	6.711664
7	$2s2p^2\ ^2D_{5/2}$	1.631400	2.116637	2.366834	2.623356	3.162142	3.783313	4.391032	6.922167
8	$2s2p^2\ ^2S_{1/2}$	2.103700	2.718146	3.031877	3.350456	4.005748	4.736238	5.396341	8.914197
9	$2s2p^2\ ^2P_{1/2}$	2.271700	2.904400	3.226615	3.554306	4.235159	5.017603	5.775246	7.777482
10	$2s2p^2\ ^2P_{3/2}$	2.279200	2.922643	3.252768	3.590666	4.295986	5.110001	5.883687	9.042412
11	$2p^3\ ^4S^o_{3/2}$	2.930000	3.769092	4.200303	4.641357	5.559413	6.570743	7.607804	11.442781
12	$2p^3\ ^2D^o_{3/2}$	3.275000	4.244846	4.739865	5.243704	6.286923	7.438014	8.565911	12.725116
13	$2p^3\ ^2D^o_{5/2}$	3.275000	4.244181	4.739318	5.243887	6.292117	7.463860	8.608740	13.002688
14	$2p^3\ ^2P^o_{1/2}$	3.699000	4.780981	5.332553	5.893711	7.053390	8.344869	9.592909	14.303522
15	$2p^3\ ^2P^o_{3/2}$	3.700000	4.782703	5.335833	5.899452	7.069656	8.388198	9.677930	14.832877

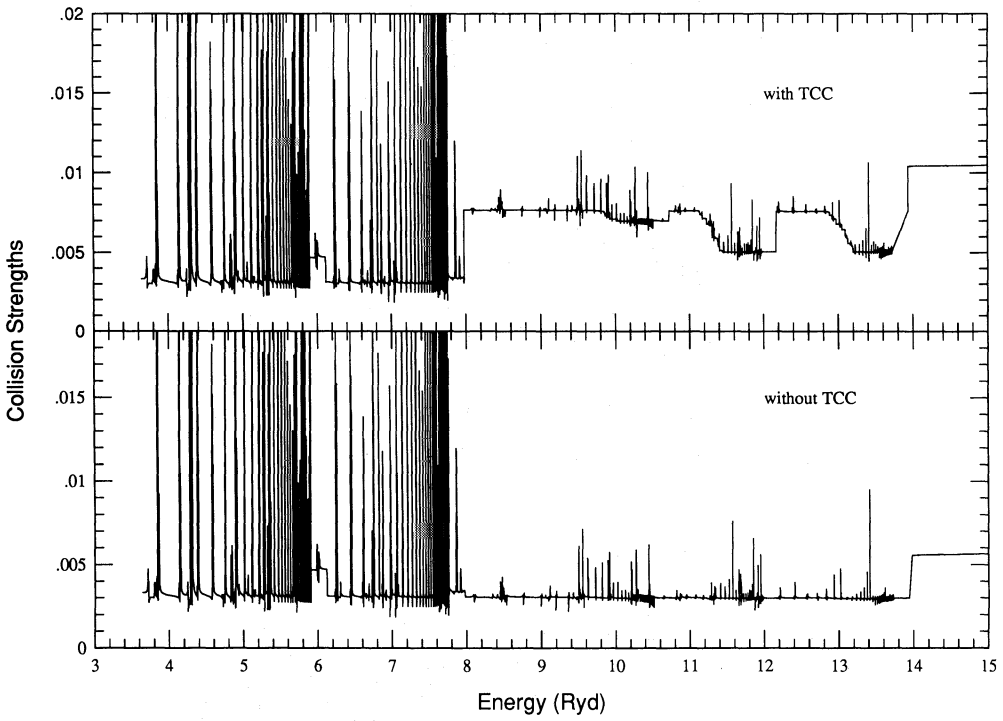

Fig. 4. The effect of relativistic term coupling on the collision strength for the transition $^2P^0_{1/2}$–$^4P_{1/2}$ in Fe XXII

(TCC), at $T = 4.41\ 10^6$ K, are $5.89\ 10^{-3}$ and $9.18\ 10^{-3}$, respectively. The relativistic effects thus enhance the rate coefficient by about 50% (detailed results will be presented in Zhang & Pradhan 1993). Our study also indicates that for $Z < 20$ the term coupling effects are not very important for the collision strengths reported. Some astrophysical applications of the present work are in progress. For example, temperature and density sensitive UV line ratios, and cooling rates for the ground state fine structure transition for all the B-like ions considered in this work, have been calculated and will be reported later (Graziani & Pradhan 1993, in preparation).

© European Southern Observatory • Provided by the NASA Astrophysics Data System

1994A&A...283..319Z

This work was supported partially by the U.S. National Science Foundation (PHY-9115057) and NASA LTSA program (NAGW-3315). The computational work was carried out on the Cray Y-MP at the Ohio Supercomputer Center in Columbus, Ohio.

References

Berrington K.A., Burke P.G., Butler K., Seaton M.J., Storey P.J., Taylor K.T., Yu Y., 1987, J. Phys. B 20, 6379
Blum R.D., Pradhan A.K., 1992, ApJS 80, 425
Burke V.M., Seaton M.J., 1986, J. Phys. B 19, L527
Eissner W., Jones M., Nussbaumer H., 1974, Comp. Phys. Comm. 8, 270
Grant I.P., McKenzie B.J., Norrington P.H., Mayers D.F., Pyper N.C., 1980, Comp. Phys. Comm. 21, 207
Hayes M.A., 1992, J. Phys. B 25, 2649
Hummer D.G., Berrington K.A., Eissner W., Pradhan A.K., Saraph H.E., Tully J.A., 1993, A&A (in press) (Paper I)
Luo D., Pradhan A.K., 1989, J. Phys. B 22, 3377
Luo D., Pradhan A.K., 1990, Phys. Rev. A 41, 165
Nahar S.N., Pradhan A.K., 1991, Phys. Rev. A 44, 2935
Osterbrock D.E., 1989, Astrophysics of Gaseous Nebulae and Active Galactic Nuclei. University Science Books, Mill Valley, CA
Pradhan A.K., 1983, Phys. Rev. A 28, 2128
Saha H.P., Trefftz E., 1982a, J. Phys. B 15, 1089
Saha H.P., Trefftz E., 1982b, Z. Naturforsch 37A, 744
Sampson D.H., Weaver G.M., Goett S.J., Zhang H.L., Clark R.E.H., 1986, ADNDT 35, 223
Seaton M.J., 1987, J. Phys. B 20, 6363
Zhang H.L., Pradhan A.K., 1993, Phys. Rev. A (to be submitted)
Zhang H.L., Sampson D.H., 1993, ADNDT (in press)

© European Southern Observatory • Provided by the NASA Astrophysics Data System